International Journal of Heat and Mass Transfer 52 (2009) 1400–1411

Contents lists available at ScienceDirect

International Journal of Heat and Mass Transfer

journal homepage: www.elsevier.com/locate/ijhmt

Mass transfer enhancement by gravity waves at a liquid–vapour interface

S.P. Das, E.J. Hopfinger *

LEGI/CNRS, B.P. 53, 38041 Grenoble, Cedex, France

ARTICLE INFO

Article history:
Received 7 April 2008
Received in revised form 20 August 2008
Available online 16 December 2008

ABSTRACT

Experimental results on mass transfer enhancement by large amplitude gravity waves at a liquid–gas/vapour interface are presented. The waves are sub-harmonically excited in a circular cylinder that is partially filled with liquid, by oscillating the cylinder in the direction normal to the liquid surface. The lowest asymmetric sloshing mode (1,1) as well as the axisymmetric mode (0,1) are considered in the limit of large fluid depth approximation and for wave amplitudes that include breaking. The fluids used are low viscosity and low surface tension liquids of low boiling point temperatures. In the mass transfer experiments the lower part of the test cell is filled with cold liquid and the upper part with gas, generally vapour, at a temperature above the saturation temperature. When the interface is at rest and the gas is vapour, the pressure decrease due to condensation is small. In the presence of large amplitude sloshing the condensation rate is large and the pressure decreases rapidly and substantially. A model is developed that expresses the pressure variation in terms of a Jacob number, interfacial temperature gradient and an effective diffusion coefficient. The effective dimensionless diffusion coefficient is the relevant similarity parameter and is determined in the experiments. In Appendix A results are presented for conditions of evaporation in the presence of a non-condensable gas.

1. Introduction

In rocket engine fuel tanks and ship tanks where the liquid fuel or liquefied gas is in contact with its vapour or a non-condensable gas, large amplitude waves can enhance condensation or evaporation at the liquid–vapour interface and cause large pressure changes. There are numerous studies of condensation–evaporation heat transfer enhancement by forced convection at walls in the context of heat exchangers [1–3] and on air–water (air–sea) gas exchange enhancement by wind forcing [4]. However, experiments on mass transfer enhancement by gravity waves at a liquid–vapour interface in closed containers are rare. Moran et al. [5] conducted mass transfer experiments in a very large-scale spherical tank, partially filled with liquid hydrogen (LH2) and pressurized to about 3 bars with gaseous hydrogen or a non-condensable gas. After filling and pressurization the tank was subjected to horizontal oscillations in the resonance frequency range. Pressure drops of the order of 1–2 bar in 10 s were measured when the interfacial sloshing amplitude was large. Lacapere [6] performed similar experiments with liquid oxygen (LOX) in a smaller, circular cylindrical tank, recording pressure drops of the order of 1 bar. It is of interest to perform experiments with, non-cryogenic, volatile liquids under laboratory conditions where experiments can more easily be controlled and repeated. By appropriate modelling of the mass transfer it is possible to determine a condensation–evaporation heat transfer coefficient that allows up-scaling of the results to larger scale containers and cryogenic liquids. This is the main objective of the present experiments conducted with FC-72 and HFE7000 liquids distributed by 3 M.

The wave modes in containers of various geometries can be found in Abramson [7] and in Ibrahim [8]. Miles [9] developed a weakly non-linear theory of wave motions in circular cylinders subjected to horizontal forcing that contains the relevant control parameters and allows determining the phase diagram of sloshing. This phase diagram is in good agreement with experiments [10]. The multimodal theory applies to fully non-linear sloshing (excluding wave breaking) and has been successfully applied to rectangular and square-base containers by Faltinsen et al. [11,12]. Large amplitude wave motions in circular cylindrical containers, including wave breaking conditions, have been investigated by Royon-Lebeaud et al. [10] focussing on asymmetric sloshing and by Das and Hopfinger [13] for axisymmetric sloshing.

Parametric forcing has the advantage that different wave modes can be excited depending on the container forcing frequency [14]. We consider here the asymmetric mode (1,1) and the axisymmetric wave mode (0,1) in a circular cylinder, where the wave modes (m,n) express m nodal diameters and $n-1+\delta_{m0}$ nodal circles with $m = 0, 1, \ldots$ and $n = 1, 2, \ldots$, where δ_{m0} is the Kronecker delta function. The liquid depth to radius ratio is known to be an important parameter because this determines the non-linear resonance. We consider only large fluid depth conditions.

* Corresponding author.
E-mail address: hopfinger@hmg.inpg.fr (E.J. Hopfinger).

0017-9310/$ - see front matter © 2008 Elsevier Ltd. All rights reserved.
doi:10.1016/j.ijheatmasstransfer.2008.08.016

Nomenclature

A	forcing amplitude
b	wave amplitude
c_{pl}	liquid specific heat
d	liquid depth
D_e	effective heat diffusivity
D_e^*	dimensionless effective heat diffusivity
D_T	liquid heat diffusivity
g	gravitational acceleration
Ja	Jacob number
k	wave number
L_{lv}	latent heat
m_v	mass of vapour
p	pressure
q_v	interfacial vapour flux
r_v	specific gas constant
R	radius of the test container
S	liquid surface
t	time
T	temperature
V	vapour volume
w_e	effective velocity normal to surface

Greek symbols

ρ	density
Θ	$T_s - T_l$
σ	surface tension
ω_f	forcing frequency
ω	wave frequency
ν	kinematic viscosity
δ	damping ratio
κ	damping rate
δ_T	thickness of the interfacial thermal boundary layer thickness in liquid

Subscripts

g	gas
h	hold
i	initial
l	liquid
r	ramp
s	saturation or boiling conditions
v	vapour

The experimental conditions and procedures are presented in Section 2 and in Section 3 the interfacial sloshing conditions with respect to the instability and wave breaking thresholds are discussed. Section 4 contains the mass transfer results. A mass transfer model is developed in Section 5 that allows comparison with other experimental conditions including the up-scaling to full-scale fuel tanks. Section 6 contains the conclusions.

2. Experimental conditions

The experiments have been conducted in a circular, cylindrical container of inner diameter $2R = 10$ cm ± 0.004 and 11.5 cm height. In the mass transfer experiments the upper half of the container is made of aluminium of 0.5 cm wall thickness and the lower half of Plexiglas, allowing the interface to be visible; the Plexiglas part has a wall thickness of 1 cm. The two halves are clammed together and are made vacuum tight by means of an o-ring seal. A schematic drawing of the whole test cell is shown in Fig. 1, containing also the locations of the thermocouples and the pressure transducer. A heating wire is wound around the upper half that allows monitoring the wall temperature. The heating power used allowed to increase the wall temperature of the upper part from room temperature (about 20 °C) to about 70 °C in 16 min. The lower part of the test cell is slightly heated by conduction from the upper half. In the isothermal experiments, for the determination of the instability and wave breaking thresholds, the upper half of the test cell is replaced by a Plexiglas cylinder of size equivalent to the lower part.

The test cell is mounted on a vertically oscillating vibration exciter, TIRA, type TV 52120 of 200 N peak force. The acceleration $a(t) = A\omega_f^2 \sin\omega_f t$, in the experiments is $a(t) \leqslant 0.2$ m/s^2 where ω_f is the circular forcing frequency and A is the forcing amplitude. After calibration the vibration amplitude could be kept within ±0.30% of the nominal value and the frequency within 0.02%. Since the vibration is normal to the fluid surface, the waves are sub-harmonically excited, that is the wave frequency $\omega = \omega_f/2$. The liquids used are FC-72, of $\nu = 0.00406$ cm^2/s, $\sigma = 11$ dyn/cm and $\rho = 1688$ kg/m^3 at 20 °C and 1 bar, $Bo = \rho g R^2/\sigma = 3768$ and HFE7000, of $\nu = 0.0031$ cm^2/s, $\sigma = 12.5$ dyn/cm and $\rho = 1415$ kg/m^3 at 20 °C.

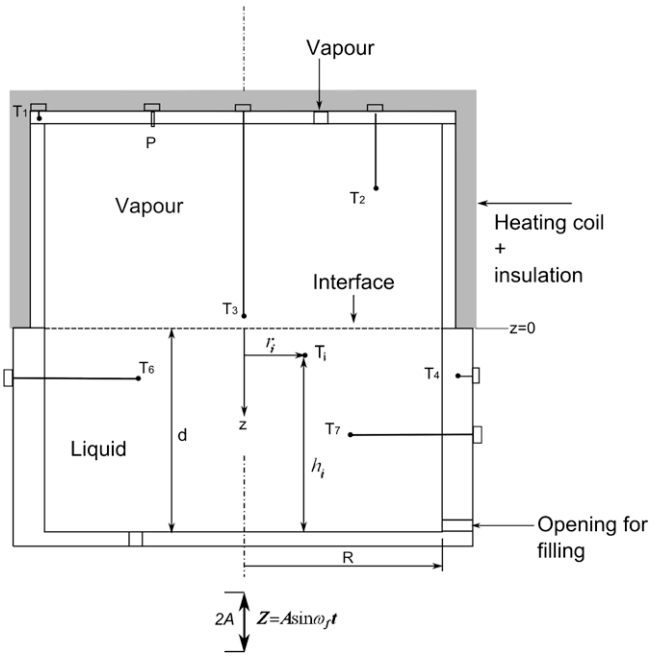

Fig. 1. Schematic of the test cell layout. The thermocouples are numbered T_i with $i = 1$–7 and are located at (h_i, r_i), i.e. at h_i cm from the bottom and at r_i cm from the center; T_1 ($h_1 = 11.6$ cm, $r_1 = 5.25$ cm) (in upper wall), T_2 (10.5, 3.3), T_3 (5.75, 0) (can be moved vertically), T_4 (5.0, 5.2) (in lower wall), T_5 (5.0, 2.5), T_6 (4.5, 2.5), T_7 (3.5, 2.5); the pressure transducer is at P (11.3, 3.3). The radius is $R = 5$ cm and the total height is 11.5 cm with the liquid surface at $d \simeq 5.5$ cm.

The boiling temperatures of these liquids are given by $T_s = 1562/(9.729 - \log_{10}(p(\text{pascal})))$ for FC-72 and $T_s = 3548.6/(22.978 - \log(p(\text{pascal})))$ for HFE7000 (from product data sheet information of 3 M). The liquid depth to radius ratio is $d/R \geqslant 1.1$ that approximates closely deep-water conditions with $\tanh(k_{01}d) \cong 1$. The liquids are fully wetting (the contact line is free to move) with a static contact angle close to zero. The thermodynamic properties of the liquids are given in Table 1, together with the properties of liquid hydrogen (LH2) and liquid oxygen (LOX) used in other experiments [5,6].

Table 1
Liquid properties. T_s and T_l are, respectively, the saturation and liquid temperatures

	M [kg/mol]	T_s [K]	ρ_l [kg/m^3]	ρ_v [kg/m^3]	L_{lv} [kJ/kg]	c_{pl} [kJ/kg K]	T_l [K]	Ja	r_v [J/kg K]	$D_T \times 10^8$ [m^2/s]
FC-72 (1 bar)	0.338	330.30	1591	12.31	84	1.10	293	63	24.6	3.06
FC-72 (2 bar)	0.338	352.76	1532	23.05	79	1.14	293	57	24.6	2.94
HFE7000 (2 bar)	0.2	329.43	1310	14.61	120	1.40	293	38	41.6	3.76
LH2 (2.5 bar)	0.002	23.77	66.35	3.08	420	12.3	20	2.4	4150	12.6
LOX (2.5 bar)	0.032	99.8	1091.7	10.3	202.1	1.73	90	8.8	260	7.3

D_T is the liquid thermal diffusivity and $Ja = \frac{\rho_l c_{pl}}{\rho_v L_{lv}}(T_s - T_l)$ is the Jacob number. The physical properties are given for temperature T_s.

Measurements of the instability and wave breaking thresholds under isothermal conditions were made by visualizations and image analysis only. Generally, a digital camera with an acquisition speed of 60 frames/s (fps) was used. Near resonant conditions with high velocity jet formation, images were also taken with a high-speed camera at 1000 fps. The thermocouples used have a precision of 0.1 °C and a response time of 0.15 s. These were calibrated in a constant temperature bath. An important point is to keep the temperature gradient along the thermocouple rod of 0.10 cm diameter as low as possible over a length of 10 rod diameters measured from the thermocouple tip. The pressure transducer is an Entran piezoelectric transducer of 50 kHz frequency response. It was calibrated in the operating pressure range 0–2.5 bar to an accuracy of 0.5 mbar. The thermocouples and pressure transducer signals were digitised at 5 Hz. The measurement times were computer monitored.

3. Instability and wave breaking thresholds

The inviscid dispersion relation with surface tension added is

$$\omega_{mn}^2 = g k_{mn}\left(1 + \frac{k_{mn}^2\sigma}{g\rho}\right)\tanh(k_{mn}d). \tag{3.1}$$

The wave numbers k_{mn} in (3.1) are obtained from the boundary condition on the container wall $\partial\phi/\partial r|_{r=R} = J'_m(k_{mn}R) = 0$, where ϕ is the velocity potential. For the axisymmetric wave mode, $m = 0$ and $n = 1$, $k_{01}R = 3.8317$ and for the lowest asymmetric mode, $m = 1$, $n = 1$, the dimensionless wave number is $k_{11}R = 1.841$. For FC-72 and $R = 5$ cm filled to a depth, $d = 5.5$ cm such that $\tanh(k_{01}d) \cong 1$ the natural frequency of mode (0,1) is $\omega_{01} = [(3.832g/R)(1 + 14.68/Bo)]^{1/2} = 27.42$ rad s^{-1} and $\omega_{11} = [(1.841g/R)(1 + 3.39/Bo)]^{1/2} = 18.72$ rad s^{-1}. The capillary contribution to the wave frequency is less than 1%.

The natural frequency shift due to linear damping is $\hat{\omega}_{01} = \omega_{01}(1 - \delta)$, where $\delta = \kappa/\omega$ is the damping ratio and κ the damping rate. The experimentally determined damping ratio for the axisymmetric mode is $\delta \approx 0.0022$ and for the asymmetric mode $\delta \approx 0.003$. The viscous correction of the frequency is, therefore, small and within experimental error. The damping occurs mainly in the stokes boundary layers (here at the side walls and is of the form

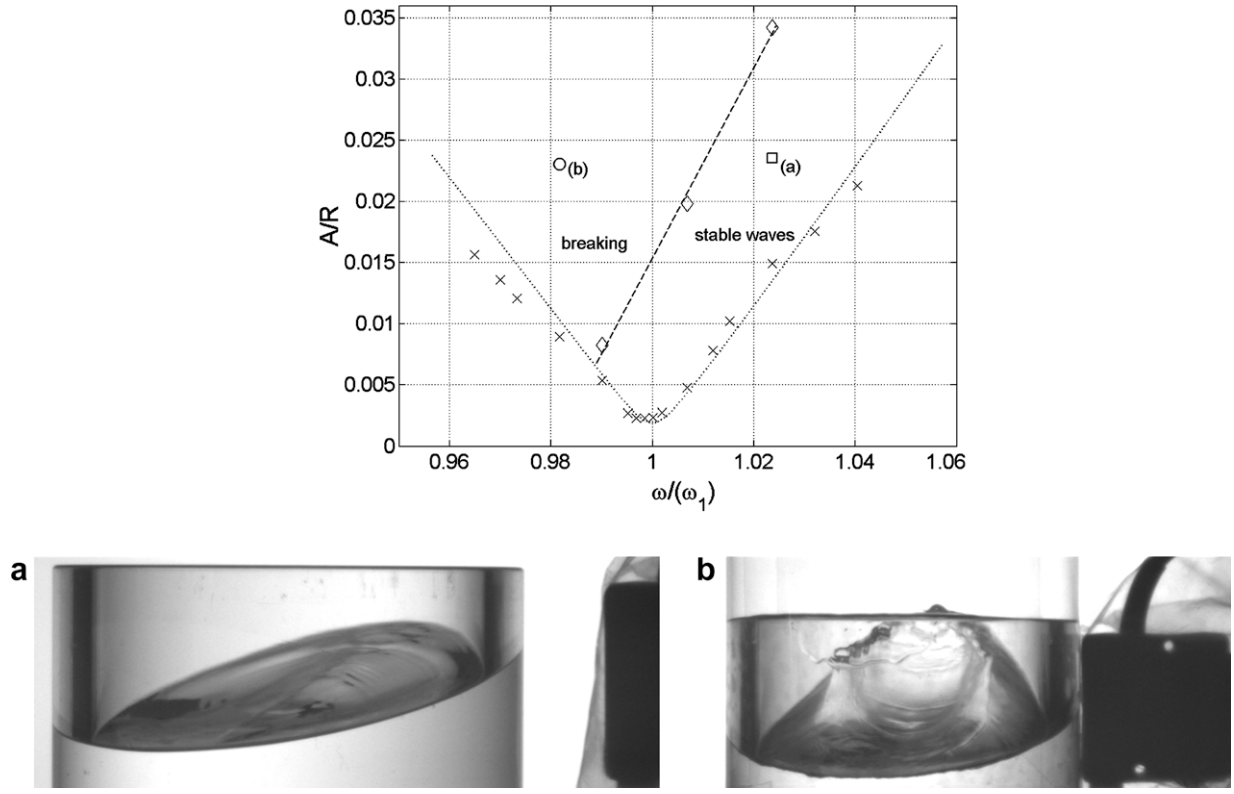

Fig. 2. Dimensionless forcing amplitude instability and wave breaking thresholds as a function of dimensionless wave frequency ω/ω_1 for the asymmetric mode (1,1) of $\omega_1 = 18.72$ rad/s ($\omega_1 \equiv \omega_{11}$). The liquid is FC-72 and the container radius $R = 5$ cm. The symbols ∘ and □ indicate the conditions of the mass transfer experiments. The images of the interfacial waves correspond to these conditions. (a) $\omega/\omega_1 = 1.0237$, $A/R = 0.0235$, $b/R = 0.40$; (b) $\omega/\omega_1 = 0.9817$, $A/R = 0.0227$, $b/R \approx 0.60$; b is wave amplitude, A is the container forcing amplitude and the forcing frequency $\omega_f = 2\omega$. Wave breaking occurs when $\omega^2 b \geqslant g$ [15], hence $b/R \geqslant 0.54$.

$\delta \sim (1/R)(\nu/2\omega)^{1/2}$). When substituting $\omega \cong \sqrt{gk_{mn}}$ we get $\delta \approx (C/\sqrt[4]{1.841})(\nu^2/gR^3)^{1/4}$ for the asymmetric mode and $\delta \approx (C/\sqrt[4]{3.832})(\nu^2/gR^3)^{1/4}$ for the axisymmetric mode. The constant $C \approx 1$.

For the asymmetric mode the instability and wave breaking thresholds are shown in Fig. 2 where the dimensionless forcing amplitude of the instability boundary is plotted as a function of wave frequency made dimensionless by the natural frequency $\omega_1 \equiv \omega_{11}$. The bounds shown in Fig. 2 have been obtained for FC-72, but the stability thresholds are practically the same for HFE7000 because the fluid properties are very similar. In any event, the main interest of Fig. 2 in the present context is to define clearly the conditions of the mass transfer experiments with respect to the stability and wave breaking boundaries. The time it takes to reach the final wave amplitudes depends on the forcing conditions. For the conditions corresponding to images (a) and (b) of Fig. 2 the times are respectively 12.2 s for (a) and 14.3 s for (b) when starting from rest. The exponential growth of the wave amplitude starts after an initial time delay; $t_i/T = 16.1$ for condition (a) and $t_i/T = 23.4$ for condition (b) where the wave period $T = 0.33$ s. In the heat transfer experiments with interface perturbations the time of growth of the wave amplitude is reduced by the initial time and is, therefore, in both cases about 7 s.

The stability and breaking thresholds of the axisymmetric mode are given in Das and Hopfinger [13]. In this case, the mass transfer experiments have been conducted for $\omega/\omega_0 = 0.9994$, $A/R = 0.008$ and $\omega/\omega_0 = 0.957$, $A/R = 0.014$ ($\omega_0 \equiv \omega_{01}$). For $\omega/\omega_0 = 0.957$, $A/R = 0.014$ jet formation occurs. Fig. 3a and b show the images of the axisymmetric stable wave and jet formation, respectively.

Fig. 3. Images of (a) stable axisymmetric wave mode for $\omega/\omega_0 = 0.9994$, $A/R = 0.008$ and of (b) composite image of jet formation (the lower part shows the cavity that collapses to form the jet or geyser), $\omega/\omega_0 = 0.957$, $A/R = 0.014$; the mass transfer experiments correspond to these conditions.

4. Mass transfer experiments

4.1. Heating and pressurization of the test cell

Most of the experiments have been conducted for conditions where condensation takes place. An experiment with evaporation is briefly presented in Appendix A. In the condensation experiments, the upper half of the test cell, made of aluminium, of total mass of 0.460 kg, is heated to a temperature a few degrees below the saturation temperature T_s at the operating pressure chosen that is close to 2 bar. For FC-72, $T_s = 352.7$ K at 2 bar (Table 1) and $T_l = 293$ K and for HFE7000, $T_s = 329.4$ K at 2 bar and $T_l = 293$ K. With the heating power of 20 W used, the heating time necessary to increase the wall temperature of the upper half by 50 °C is 16 min (required in the case of FC-72) and 8 min required to increase the upper part by 30 °C, needed in the experiments with HFE7000. The rate of increase (by conduction) of the wall temperature of the lower part of the test cell, at location of temperature probe T_4, is 0.0017 °C s^{-1}. The regulated power supplied to the heating coil is on average about 26 W with a higher value in the beginning and less at the end when the required temperature is approached.

After the desired temperature has been reached, the air in the test cell and supply lines has been evacuated to an absolute pressure of about 75 mbar. The time origin in Fig. 4 is the time when the evacuation has been stopped. After a few tens of seconds, the cold liquid (the liquid is passed through a cooling coil) is slowly supplied from below, giving rise to a pressure increase due to boiling and evaporation with a small contribution due to compression of the remaining, non-condensable gas (air) in the test cell. The contribution of the gases dissolved in the liquid (48 ml per 100 ml liquid) is insignificant. Fig. 4a shows the pressure evolution during liquid filling and pressurization for FC-72 with the corresponding temperatures shown in Fig. 4b. When the liquid level has nearly reached the desired height, (in about 300 s in the experiments) the pressure is ramped up during about 40 s to the operating pressure of about 2 bar by injecting vapour at a temperature above the saturation temperature. In order to avoid impingement of the vapour jet on the liquid surface, the vapour is injected in the radial direction just below the top wall of the test cell. The liquid surface is maintained at about 5.5 cm from the bottom with small variations occurring due to condensation during vapour injection. The pressure and temperature evolutions during the filling and ramping procedures for HFE7000 (similar to the experiments with FC-72) are shown in Fig. 4c and d.

4.2. Pressure drop due to asymmetric sloshing (asymmetric wave mode)

After a hold time of about 20–30 s after ramping has been completed, liquid sloshing has been initiated by switching on the vibrator at the desired amplitude and frequency, here for the

asymmetric sloshing mode. There is, generally, a small pressure variation during the hold phase while the wall temperature and the injected vapour temperature adjust. This depends somewhat on the time when the vapour supply valve is closed with respect to the end of the hold phase. The forcing frequencies and forcing amplitudes imposed are $\omega/\omega_1 = 1.0237$; $A/R = 0.0235$ for stable wave motion (□ in Fig. 2) and $\omega/\omega_1 = 0.9817$; $A/R = 0.0227$ for wave breaking conditions (○ in Fig. 2). In order to verify the dependency on wave amplitude, an additional experiment was conducted for $\omega/\omega_1 = 1.0069$ and $A/R = 0.0102$. Pressure and temperature variations as a function of time, with the origin of time taken at the beginning of ramping (see Fig. 4) are shown in Fig. 5. Sloshing is maintained for 100 s. When sloshing is started the heating of the upper part of the test cell was switched off. Note also that it takes about 5–10 s (depending on initial perturbations) for the wave amplitude to grow to the nominal value.

Fig. 5a shows the pressure drop for FC-72 for breaking and stable waves; for breaking waves (Δ in Fig. 5a) the rate of pressure decrease is nearly an order of magnitude higher than the value in the case of stable wave motion (× in Fig. 5a). The behavior is similar for HFE7000 (Fig. 5c). As expected, the rate of pressure drop is largest in the beginning (after the wave amplitude has reached the nominal value, after about 7 s) and is $\partial p/\partial t = 41$ mbar/s for HFE7000 in the wave breaking experiments compared with $\partial p/\partial\, t = 5.4 mbar/s$ for stable wave sloshing.

The corresponding temperature evolutions are shown in Fig. 5b for FC-72 and in Fig. 5d for HFE7000. During sloshing the vapour temperature decreases and the liquid temperature increases. Part of the increase in liquid temperature is due to heat transfer from the wall as the liquid (in the case of the asymmetric sloshing mode) moves up the hot wall of the upper part of the test cell.

4.3. Pressure drop due to axisymmetric wave mode and jet formation (geysering)

Fig. 6a and b show, respectively, the pressure and temperature variations for FC-72 and Fig. 6c and d for HFE7000 for axisymmetric sloshing motion. It is seen that the rate of pressure drop in the case of stable axisymmetric wave motion, $\omega/\omega_0 = 0.9994$, $A/R = 0.008$ (see Fig. 3), is considerably less than in the case of the stable asymmetric wave mode and is practically identical to the rate of pressure drop at an undisturbed interface. However, in the case of jet formation (geysering), $\omega/\omega_0 = 0.957$, $A/R = 0.014$, the rate of pressure drop is very large. It is important to note that the pressure decrease stops rapidly because the forcing is switched off right after geyser formation. The reason for doing this is be-

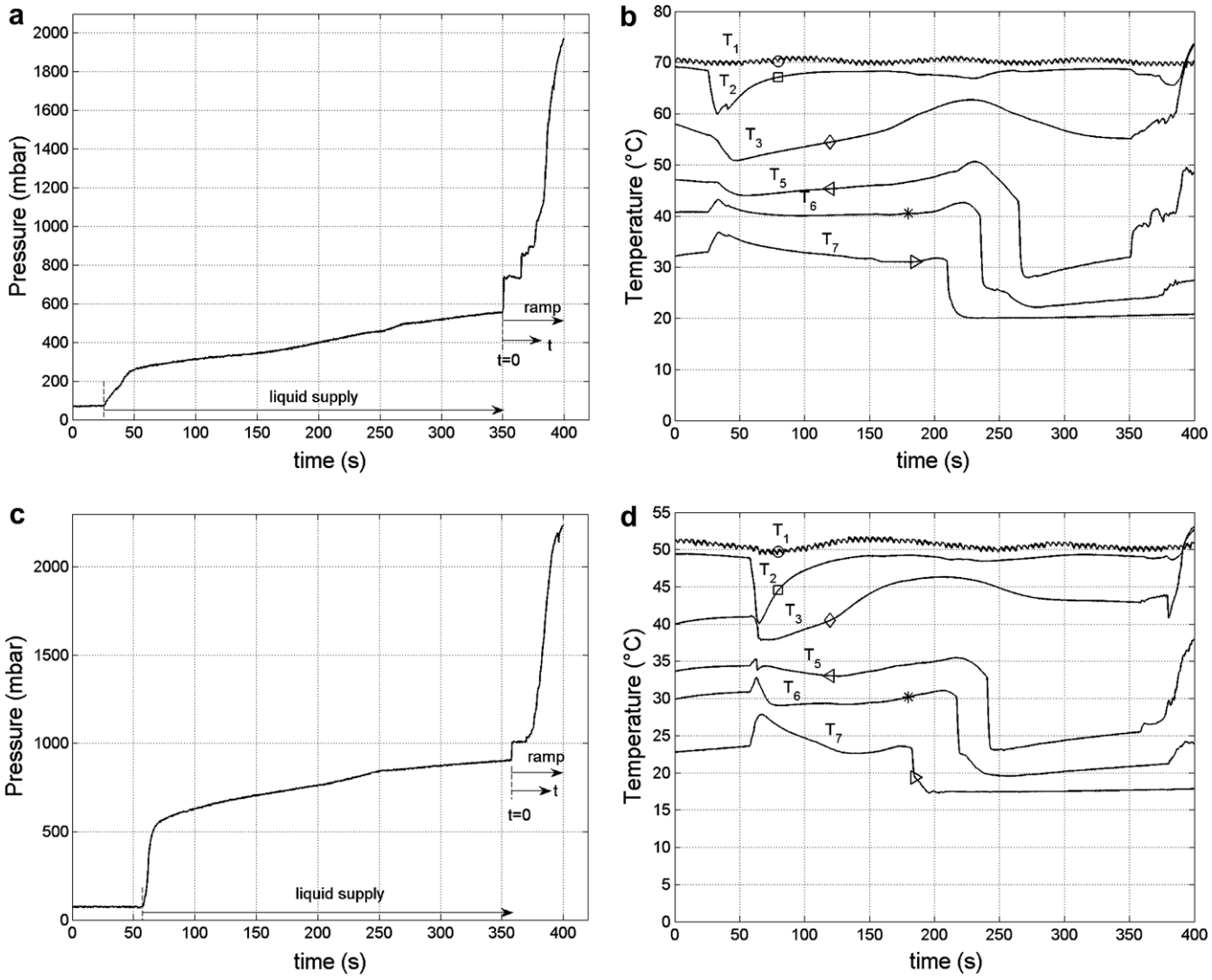

Fig. 4. Pressure and temperature variation during liquid supply and pressure ramp-up by vapour injection: (a) and (b) for FC-72 and (c) and (d) for HFE7000. The time origin $t = 0$ at the beginning of the ramping, indicated in (a) and (c), correspond the time origins in Figs. 5 and 6.

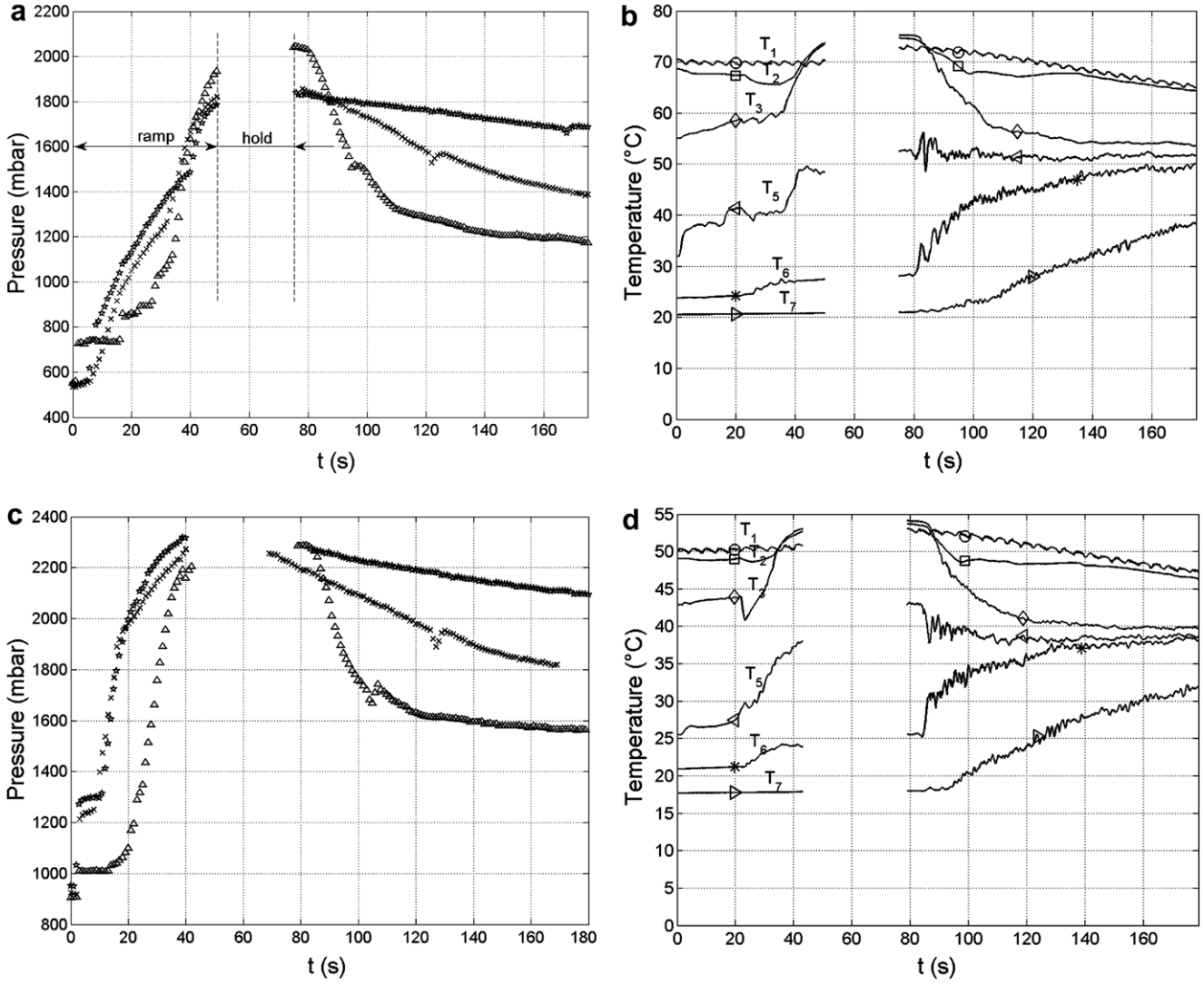

Fig. 5. Pressure and temperature variations as a function of time during ramping, hold and asymmetric sloshing: (a) and (b) for FC-72; (c) and (d) for HFE7000. Symbols △, × and ☆ in (a) and (c) are, respectively, for wave breaking regime ($\omega/\omega_1 = 0.9817$, $A/R = 0.0227$), stable regime ($\omega/\omega_1 = 1.0237$, $A/R = 0.0235$) and molecular diffusion without any interfacial motion. In (b) and (d) the corresponding temperature distributions at different locations of the container are shown for the wave breaking regime ($\omega/\omega_1 = 0.9817$, $A/R = 0.0227$). Time can be made dimensionless by the wave period $2\pi/\omega_1 = 0.33$ s.

cause in applications a geyser may form at engine restart after a low gravity flight and there is no further forcing of the liquid motion. The pressure drop continues until the decaying axisymmetric wave has reached a sufficiently small value after about 20 wave periods. The sharp decrease in temperature at location of the temperature probe T_3 is due to the sudden emergence of the liquid jet.

4.4. Analysis of the rate of pressure drop

The important quantity is the rate of pressure drop which is given by the slope of pressure change as is indicated in Fig. 7 for sloshing with breaking ($\omega/\omega_1 = 0.9817$, $A/R = 0.0227$) of FC-72 and HFE7000. The rate of pressure drop for all experiments is summarized in Table 2.

From the rate of pressure drop the vapour condensation rate can be determined. The pressure is given by

$$p = r_v \frac{m_v}{V} T_v + r_g \frac{m_g}{V} T_g, \tag{4.1}$$

where the vapour and gas temperatures at the start of sloshing, that is after pressure ramping and hold, are $T_v = T_g = T_i$, V is the vapour (gas) or ullage volume, $m_v = \rho_v V$ and $m_g = \rho_g V$ are, respectively, the vapour and non-condensable gas masses. The non-condensable gas pressure can be determined from the initial conditions (see Fig. 4a)

$$p_{g0} = r_g \frac{m_g}{V_0} T_0 \tag{4.2}$$

where V_0 is the total container volume. The initial partial pressure of the non-condensable gas is, therefore, $p_g = p_{g0} \frac{V_0}{V} \frac{T_i}{T_0}$ and the initial vapour pressure is $p_{vi} = p_i - p_g$. The rate of pressure change is then given by

$$\frac{\partial p}{\partial t} = \frac{r_v}{V} T_i \frac{\partial m_v}{\partial t} + \frac{p_i}{T_i} \frac{\partial T_v}{\partial t} \tag{4.3}$$

with the rate of change in vapour mass

$$\frac{\partial m_v}{\partial t} = \rho_v S q_{vs} + \rho_v S_w q_w \tag{4.4}$$

where S is the liquid surface area, S_w the cold wall surface in contact with the vapour during sloshing, q_{vs} is the rate of change of vapour volume per unit liquid surface and q_w the rate of change of vapour volume per unit wall surface. The contribution of the condensation at the wall depends on the sloshing mode and on the upper wall temperature conditions. Since in the present experiments the upper

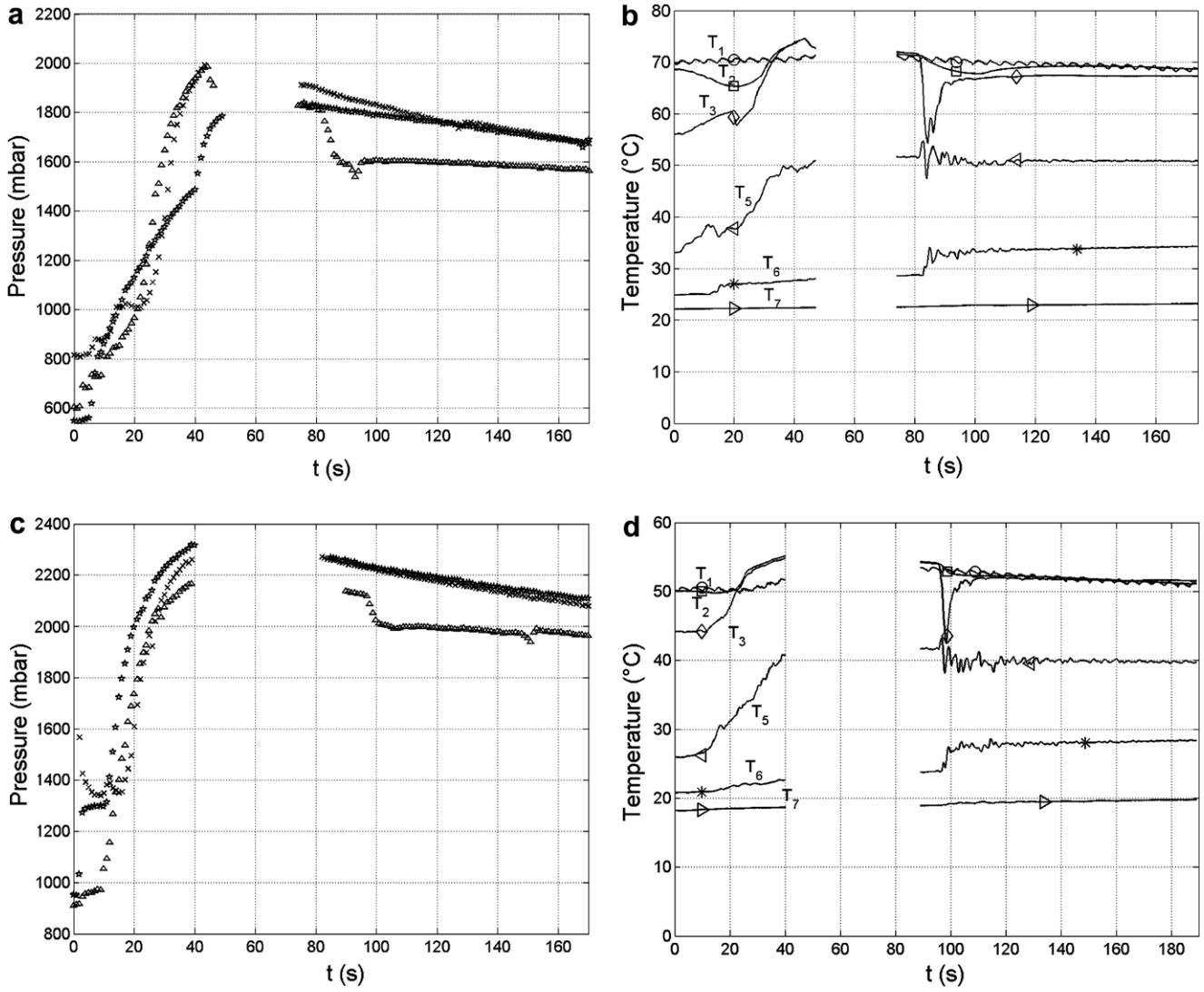

Fig. 6. Pressure and temperature variations with time during ramping, hold and axisymmetric sloshing: (a) and (b) for FC-72; (c) and (d) for HFE7000. Symbols △, × and ☆ in (a) and (c) are, respectively, for jet formation ($\omega/\omega_1 = 0.9994$, $A/R = 0.008$), stable axisymmetric wave ($\omega/\omega_1 = 0.957$, $A/R = 0.014$) and molecular diffusion without any interfacial motion. (b and d) The corresponding temperature variations at different locations of the container. The wave period is $2\pi/\omega_1 = 0.23$ s.

wall is hot (below, but close to T_s) and is not much cooled down when the liquid moves up the wall, there is little condensation. However, condensation takes place on the lower cold wall as the interface moves down and up during the sloshing motion. The maximum downward motion in the asymmetric sloshing mode is less than $0.5R$ [10]. Therefore, the cold wall surface S_w in contact with the vapour is less than about $0.2S$. Furthermore, the condensed vapour will end up at the liquid surface. For this reason, and because no separation of the respective contributions is possible, we group the two contributions together to $\frac{\partial m_v}{\partial t} = \rho_v S q_v$. The rate of change in vapour volume is then given by

$$q_v = \frac{(\partial p/\partial t) - (p_i/T_i)\partial T_v/\partial t}{r_v \rho_{vi} T_i}\left(\frac{V}{S}\right) \tag{4.5}$$

The denominator is $r_v\rho_{vi}T_i = p_{vi}$. In the present experiments $V/S \cong 60$ mm and the other experimental values are given in Table 2.

Table 2 shows that the condensation rate in the stable sloshing regime is considerably less than in the resonant sloshing regime when wave breaking and chaotic motions occur. In the stable asymmetric wave regime (second line in Table 2) the wave amplitude is $b \simeq 2$ cm and $D_e^* = 2.17 \times 10^{-6}$. An experiment with about half this wave amplitude, $b \simeq 0.78$ cm (line 3 in Table 2) gives a considerably smaller value, $D_e^* = 1.07 \times 10^{-6}$. As will be argued in Section 5, we expect the effective diffusion coefficient $D_e' = D_e - D_T$ to scale with ωb^2. For the two experiments (lines 2 and 3) the ratio of ωb^2 is 6.6 which is close to the ratio of the measured effective diffusion coefficients D_e' (the ratio is 6). As will be seen in Section 5 below, D_e^* should not depend on the fluid properties except for the difference of D_T. The values of D_e^* in Table 2 for the two fluids should, therefore, be nearly the same for the same sloshing conditions. This is the case for the stable wave conditions but there is some difference for the breaking wave conditions. This is attributed to experimental uncertainty in the wave breaking experiments with chaotic sloshing. Also, in the case of FC-72 the wall is heated to a higher temperature with more heat conduction to the lower half of the container containing the cold liquid. When taking into account these aspects, the agreement can be considered acceptable with D_e^* being given to ±12%.

4.5. Temperature profiles

The temperature profiles in the liquid and vapour phase before and after ramping and after sloshing in the wave breaking mode are shown in Fig. 8. The horizontal dotted lines indicate the li-

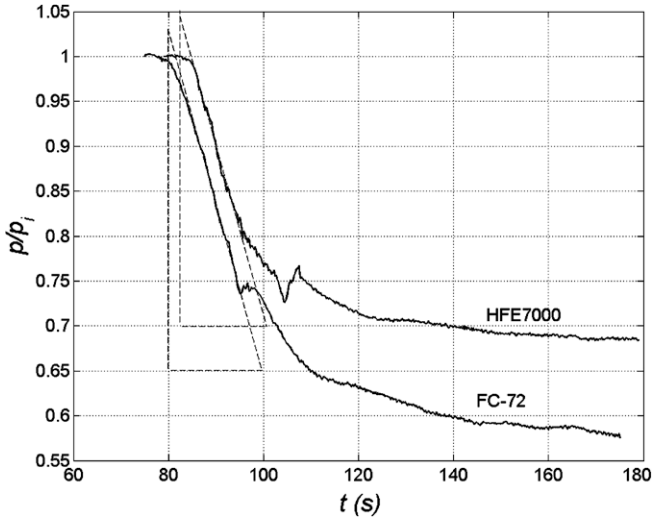

Fig. 7. Example of the rate of pressure drop during asymmetric sloshing for FC-72 and HFE7000 ($\omega/\omega_1 = 0.9817$, $A/R = 0.0227$). The kinks in the pressure drop curves (here at about $t = 95$ and 104 s) are caused by an anomalous behavior of the pressure transducer; it does not affect the results in any way.

quid–vapour interface after ramping. The liquid depth increases by about 0.2 cm during ramping due to vapour condensation at the liquid surface and at the walls. This condensation causes an agitation and consequent temperature homogenisation at the liquid surface. Consequently, the temperature gradient near the liquid surface is reduced. As will be shown below, the temperature gradient right at the liquid surface is an essential parameter in the condensation process.

The temperature profiles show that after ramping the temperature in the vapour phase is nearly uniform and is denoted as T_i in (4.5). In the liquid the temperature is also uniform over most of the depth except in the interfacial zone where over about 1 cm a sharp temperature increase occurs. After sloshing, the temperature in the vapour is decreased and increased in the liquid layer with the temperature gradient extending nearly over the whole liquid depth.

5. An interfacial mass transfer model

5.1. Effective diffusion coefficient

The thermal energy equation for the liquid phase, time averaged over a wave period, can be written in the form

$$\rho_l c_{pl}\left(\frac{\partial T}{\partial t} + w_e\frac{\partial T}{\partial z}\right) = \rho_l c_{pl} D_T \frac{\partial^2 T}{\partial z^2} \tag{5.1}$$

where z is taken positive downward into the liquid with $z = 0$ at the liquid surface and w_e is a effective velocity normal to the surface. The other variables are given in Table 1. An important aspect is the existence of two time scales, one short, corresponding to the wave period and the other long at which the mass transfer occurs. On the short time scale a distortion of the temperature gradient occurs due to the sloshing motion but the temperature gradient, integrated over a wave period, is in the vertical, z direction only.

The convective term (second term on the left hand side) in (5.1) is modelled by a gradient diffusion hypothesis [16] in the form:

$$\rho c_{pl} w_e \frac{\partial T}{\partial z} = -\rho c_{pl} D'_e \frac{\partial^2 T}{\partial z^2} \tag{5.2}$$

Equation (5.1) is thus written as

$$\rho_l c_{pl}\frac{\partial T}{\partial t} = \rho_l c_{pl} D_e \frac{\partial^2 T}{\partial z^2}. \tag{5.3}$$

where $D_e = D'_e(1 + D_T/D'_e)$ is an effective diffusion coefficient. At a motionless interface we have $D'_e = 0$, hence $D_e = D_T$. Note that D_e/D_T is a Nusselt number. Integration of Eq. (5.3) from $z = 0$ (interface position) to $z = d$ (bottom of liquid column) gives.

$$\frac{\partial}{\partial t}\int_0^d T\,dz = -D_e\left.\frac{\partial T}{\partial z}\right|_{z=0} \tag{5.4}$$

The boundary condition at the interface $z = 0$ is given by the vapour flux q_v, which is positive in the case of evaporation of liquid and negative when vapour is condensed. The expression of this boundary condition is

$$\rho_l c_{pl} D_e \left.\frac{\partial T}{\partial z}\right|_{z=0} = \rho_v L_{lv} q_v \tag{5.5}$$

The temperature gradient in the liquid surface layer is expressed by

$$\left.\frac{\partial T}{\partial z}\right|_{z=0} = -\frac{\Theta}{\delta_T} \tag{5.6}$$

where $\Theta = T_s - T_l$, with T_s the boiling or saturation temperature and T_l the bulk liquid temperature. The interfacial vapour flux is thus given by

$$q_v = -\frac{D_e}{\delta_T}\frac{\rho_l c_{pl}}{\rho_v L_{lv}}\Theta \tag{5.7}$$

where $Ja = \frac{\rho_l c_{pl}}{\rho_v L_{lv}}\Theta$ is the Jacob number. It is recognized that $\rho_l c_{pl} D_e/\delta_T$ is known as the condensation–evaporation heat transfer coefficient [3].

The vapour flux q_v is determined experimentally from Eq. (4.5) for known sloshing conditions, expressed by D_e, thermodynamic conditions, expressed by Ja and the temperature gradient at the interface, expressed by δ_T. One of the objectives of the present experiments has been the determination of the effective diffusion coefficient D_e that can then be used to predict condensation and evaporation rates for other fluids and container sizes. This diffusion coefficient is according to (5.7) given by

$$D_e = D'_e(1 + D_T/D'_e) = -q_v\frac{\delta_T}{Ja} \tag{5.8}$$

In order to make D_e representative of sloshing in different size containers, it is necessary to normalize D_e by appropriate velocity and length scales or time and length scales. The velocity scale is ωb that is proportional to $\sqrt{aR}$ where a is the axial acceleration, equal to the gravitational acceleration g in the laboratory. For the length scale we have the choice of taking the wave amplitude b that is proportional to the container radius R, or taking the thermal Stokes boundary layer thickness $\delta_S \sim (D_T/\omega)^{1/2} \sim (\nu/\omega)^{1/2}\mathrm{Pr}^{-1/2}$. Since $\delta_s \gg \delta_T$ it is unlikely that δ_s is here the relevant scale (it is the appropriate scale on the container wall). The wave amplitude b, proportional to the container radius for given sloshing conditions, is characteristic of the straining of the liquid surface layer by the sloshing motion causing a thinning of the thermal boundary layer. Therefore, we take as the characteristic scales $\sqrt{gR}$ and R. With these scales we get for the dimensionless, effective diffusion coefficient

$$D^*_e = D'^*_e(1 + D_T/D'_e) = -q_v\frac{\delta_T}{Ja}\frac{1}{(gR^3)^{1/2}} \tag{5.9}$$

The temperature gradient in the liquid surface layer is given by $\delta_T = C(D_T(t_r + t_h))^{1/2} + \delta_{Ti}$ with C of order 1 (we take $C = 3$ by analogy with momentum diffusion) and δ_{Ti} depending on the filling conditions. Substituting for δ_T in (5.9) gives

$$D^*_e = D'^*_e(1 + D_T/D'_e) = -q_v\frac{3(D_T(t_r + t_h))^{1/2} + \delta_{Ti}}{Ja(gR^3)^{1/2}} \tag{5.10}$$

Table 2
Summary of the experimental conditions and results

Liquid	Mode	ω/ω_1	A/R	p_i [mbar]	p_g [mbar]	$\partial p/\partial t$ [mbar/s]	Δp [mbar]	$\partial T_v/\partial t$ [K/s]	$q_v \times 10^2$ [cm/s]	$D_e^* \times 10^6$
FC-72	(1,1)	0.9817	0.0227	2042	133	−42	870	−0.375	−12	13.4
FC-72	(1,1)	1.0237	0.0235	1855	136	−6.52	478	−0.10	−2.1	2.17
FC-72	(1,1)	1.0069	0.0102	2131	148	−3.5	229	−0.056	−0.95	1.07
HFE7000	(1,1)	0.9817	0.0227	2288	144	−41	727	−0.403	−11.4	16.6
HFE7000	(1,1)	1.0237	0.0235	2255	136	−5.40	440	−0.071	−1.4	2.21
FC-72	(0,1)	0.9570	0.014	1829	163	−42.01	292	−0.40	−14.4	15.8
FC-72	(0,1)	0.9994	0.008	1912	137	−4.2	253	−0.06	−1.3	1.40
FC-72	–	–	–	1838	150	−2.5	213	−0.03	−0.83	0.85
HFE7000	(0,1)	0.9570	0.014	2135	140	−43.5	214	−0.50	−12.1	19.3
HFE7000	(0,1)	0.9994	0.008	2270	142	−3.33	210	−0.035	−0.9	1.45
HFE7000	–	–	–	2268	163	−2.5	180	−0.04	−0.65	1.07
HFE7000	(1,1)	0.9817	0.0227	2350	1975	+38	+400	–	+59	42

The vapour condensation rate is calculated from (4.5) and the dimensionless effective diffusivity from (5.10) with δ_{Ti} = 1.75 cm for FC-72 and δ_{Ti} = 1.6 cm for HFE7000. The dimensionless molecular thermal diffusivities in the table are $D_T^* = D_T/(gR^3)^{1/2} = 0.85 \times 10^{-6}$ for FC-72 and 1.07×10^{-6} for HFE7000.

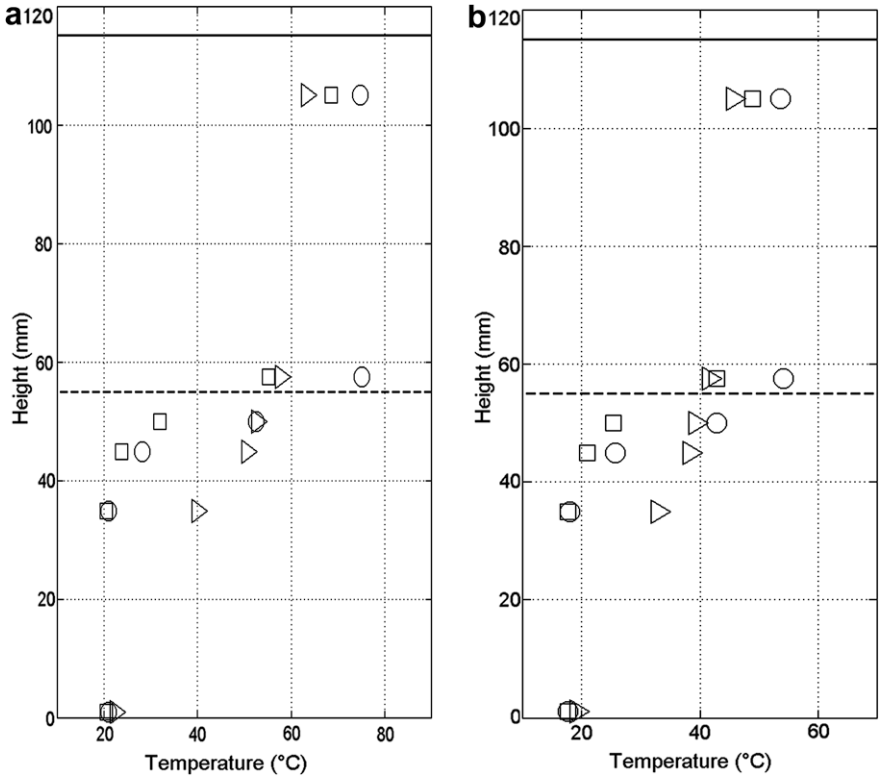

Fig. 8. Temperature distribution along the height with the origin taken at the bottom of the container; □, before ramping; ○, after ramping; ▷, after the asymmetric sloshing experiments. (a) FC-72, ω/ω_1 = 0.9817, A/R = 0.0227 and (b) HFE7000, ω/ω_1 = 0.9817, A/R = 0.0227. The horizontal dashed line and solid line indicate the interface position after ramping and the location of the top wall, respectively.

$D_e'^*$ characterizes the sloshing regime (stable or breaking); in the stable wave regime the value of $D_e'^*$ depends on dimensionless frequency and on dimensionless forcing amplitude which determine the wave amplitude. In the breaking or chaotic (resonant) sloshing regime the forcing amplitude is less important. The experimental value of $D_e^* = D_e'^*(1 + D_T/D_e')$ is given in Table 2, calculated with δ_{Ti} = 1.75 cm for FC-72 and δ_{Ti} = 1.6 cm for HFE7000. These values of δ_{Ti} have been determined from the pressure change due to molecular diffusion alone at the motionless interface. Because of the condensation at the cold liquid surface and the container walls during ramping, a thin mixed layer forms near the surface causing a decrease in the interfacial temperature gradient.

5.2. Comparison with other experiments

It is of interest to use the present results together with the transfer model to predict the pressure drop in the large-scale experiments of Moran et al. [5]. These authors used liquid hydrogen (LH2) at 2.5 bar in a large spherical container of R = 74.8 cm. In the asymmetric sloshing regime where wave breaking occurs, a pressure drop of more than 1 bar in 10 s has been measured. In Table 3 we compare the values predicted by up-scaling of the present experimental results to the experimental conditions of Moran et al. [5]. For a similar sloshing regime (wave breaking) we determined from the present experiments $D_e'^* \approx 15.5 \times 10^{-6}$ (for HFE700). This gives an effective, dimensional diffusion coefficient in the experiments of Moran et. al. of $D_e = D_e'^*(gR^3)^{1/2} + D_T \approx 316 \times 10^{-3}$ cm^2/s. The vapour condensation rate q_v is then calculated from (5.10) using the values for LH2 at 2.5 bar that are given in Table 1. Forδ_T we use $\delta_T \approx 3((D_T(t_r + t_h))^{1/2}$. Because of the lower thermal inertia of the walls in the large-scale experiment with LH2, mixing at the liquid surface due to condensation at the container wall during ramping is likely to be insignificant, hence we take $\delta_{Ti} \approx 0$.

Table 3
Comparison of predicted pressure change for LH2 with the experimental value of Moran et al. [5] and the LOX experiments of Lacapere [6]

	R [cm]	p_i [bar]	T_i [K]	$t_r + t_h$ [s]	$\frac{p_i}{T_i}\frac{\partial T_v}{\partial t}$ [mbar/s]	$\frac{\partial p}{\partial t}$ [mbar/s]	q_v [cm/s]	δ_T [cm]	$D_e \times 10^3$ [cm^2/s]	$D_e'^* \times 10^6$
HFE7000 (2.2 bar)	5	2.2	327	79	−2.8	−41	−0.11	2.1	5.8	15.5
LH2 (2.5 bar)	74.8	2.5	40	50	−92	$(-175)_{exp}$ $(-160)_c$	$(-1.01)_c$	$(0.75)_c$	316	15.5
LOX (2.5 bar)	9.1	2.5	110	87	−28	$(-83)_{exp}$ $(-40)_c$	$(-0.16)_c$	$(0.75)_c$	14.1	15.5

The sloshing regime is characterized by D_e^* determined from the present experiments and used to predict the pressure changes in the other experiments. The vapour condensation rate is given by (5.9). The total pressure change is composed of the vapour condensation rate and the vapour temperature change (4.5). Note that $D_e = D_e'^*(gR^3)^{1/2} + D_T$. Subscript c stands for calculated and exp for measured.

The rate of change of the pressure is calculated from (4.5) that includes the pressure change due to the vapour temperature change evaluated from the experiments of Moran et al. to $\Delta T_v/\Delta t \approx 29$ K/11 s. It may be noted that in the present experiments the contribution to the pressure change of the vapour temperature change is small mainly because the absolute temperatures are large. As is seen in Table 3, there is fairly good agreement between the pressure drop measured by Moran et al. of $\frac{\partial p}{\partial t} \approx -175$ mbar/s and the predicted value of $\partial p/\partial t \approx -160$ mbar/s, considering that in the Moran et al. experiments the container is spherical and is laterally forced with large forcing amplitude ($A/R = 0.05$) causing wave breaking to be more violent [10] than in the present parametrically forced case where $A/R = 0.023$. It is also possible that the cold liquid that moves up the container wall will cool the wall and hence cause some vapour condensation at the wall as well. Furthermore, the pressure drop given in Table 3 is the largest value of the 25 experimental runs of Moran et al. The uncertainty in the prediction is the initial temperature gradient in the liquid surface layer expressed by δ_T; the condensation rate, and hence the pressure change, is inversely proportional to δ_T.

In the experiments by Lacapere [6] LOX was pressurized to 2.5 bar with oxygen vapour in a glass cylinder of $R = 9.1$ cm and 80 cm height. In the experiment, included in Table 3, the ullage volume was about $V = 7.8$ l ($V/S \simeq 35$ cm). A pressure drop of about 1 bar in 12 s was measured. The decrease in vapour temperature can be estimated to be from about 110 to 95 K in 12 s. Since the cylinder is made of glass (low thermal inertia) and is vacuum insulated we take $\delta_{Ti} = 0$. The predicted pressure drop is only about half the measured value. The discrepancy may be due to the very large lateral forcing amplitude used in these experiments ($A/R = 0.26$) causing very chaotic sloshing.

6. Conclusions

It is shown that large amplitude interfacial waves increase substantially the heat and mass transfer at the liquid–gas interface. Here, mass transfer by vapour condensation is emphasized with an example of evaporation given in Appendix A. The interfacial motion enhances and distorts the temperature gradient, hence increasing the effective diffusivity. A model is developed showing that the vapour condensation (evaporation) rate depends essentially on three parameters: the Jacob number Ja that contains the thermodynamic properties of the fluid, the temperature gradient in the liquid surface layer, characterized by δ_T and the liquid sloshing motion expressed by an effective diffusion coefficient D_e. When the interface is motionless, this effective diffusion coefficient is identical to the molecular thermal diffusivity D_T in the liquid phase. The ratio D_e/D_T is, therefore, a Nusselt number.

It is shown that the effective diffusivity depends on the interfacial velocity given by ωb and on the wave amplitude b, both causing a straining of the interfacial thermal boundary layer. Thus the effective diffusivity scales with ωb^2. Since sloshing occurs in the neighbourhood of the resonant frequency (otherwise wave amplitudes remain small). We can express ω in terms of the axial fluid acceleration and the container radius $\omega \propto \sqrt{g/R}$ or, more generally $\omega \propto \sqrt{a/R}$ when a differs from g. The wave amplitude is proportional to R for similar forcing conditions. The effective diffusion coefficient is, therefore, made dimensionless by $(gR^3)^{1/2}$, that is $D_e^* = D_e/(gR^3)^{1/2}$. This dimensionless diffusion coefficient, or more precisely $D_e'^* = D_e^*(1 - D_T/D_e)$ because the sloshing motion does not affect the molecular diffusion, is the similarity parameter. The Bond and Reynolds numbers are assumed to be large which is the case in the laboratory experiments and in applications. The values of D_e^* determined in the present experiments can be used to calculate the pressure change for similar sloshing conditions in containers of different sizes and for different fluids. Two examples, one for LH2 in a large container and the other for LOX, have been given in Table 3. The uncertainty in doing this is the temperature gradient in the liquid surface layer characterized by δ_T.

Usually, the Nusselt number, here $Nu = D_e/D_T$, is expressed in terms of a control parameter. In the problem considered, the primary parameter would be b/R and up to wave breaking the relation would be $Nu \sim (b/R)^2$ and then it would probably increase more slowly with forcing amplitude A/R because the wave growth-collapse cycle is more rapid, leading to a more chaotic state of sloshing. Since the wave amplitude b is not an explicit parameter and does not depend in a simple way on dimensionless forcing amplitude and forcing frequency, we did not present the results in this form.

Acknowledgements

The valuable technical help of Pierre Carecchio and Joseph Virone is gratefully acknowledged. The work was financially supported by contract CNES No. 60167 within the COMPERE program. The work profited considerably from discussions within the COMPERE working group.

Appendix A. Pressure change due to evaporation

It is of interest to show that the mass transfer model also applies to evaporation at the liquid–gas interface. For evaporation to take place, the liquid surface has to be heated to a temperature above the boiling temperature by the hot gas above and by the hotter liquid below. This heat flux is given by

$$j = j_g + j_l = \kappa_g(T_s - T_{g0})/\delta_{Tg} + \kappa_l(T_s - T_{l0})/\delta_{Tl}. \quad \text{(A1)}$$

Since the ratio of the thermal conductivities $\kappa_g/\kappa_l \ll 1$ and $\delta_{Tg}/\delta_{Tl} \gg 1$ (much larger thermal diffusivity of the gas), the liquid surface heating by the gas is negligible except when $(T_s - T_{l0}) \approx 0$ (when the partial pressure of the vapour has appreciably increased) in which case evaporation is negligible. It is, therefore, justified to analyse the evaporation results in terms of the model developed in Section 5.

The evaporation experiments have been conducted with air as non-condensable gas and HFE7000. The test cell was heated at 1 bar (opening to the atmosphere) to a temperature of about 55 °C. Then, the communication with the atmosphere was closed

and liquid injection was started. Fig. A1 shows the pressure (a) and temperature changes (b) during liquid injection and hence compression of the gas (air) in the test cell as a function of time. The pressure at the end of the filling, at 300 s in Fig. A1, is composed of

$$p = p_g + p_v = r_g \frac{m_g}{V} T_g + r_v \frac{m_v}{V} T_v \tag{A2}$$

where $T_g = T_v$ and $p_g = p_{g0} \frac{V_0}{V} \frac{T_g}{T_{g0}}$ where $V_0/V \simeq 1.92$ and from Fig. A1b, $T_g/T_{g0} \approx 1.03$. The non-condensable gas pressure in Fig. A1a is, therefore, $p_g \simeq 1975$ mbar which gives a vapour pressure at the end of liquid supply of $p_v = p - p_g$. The temperature evolutions at the different thermocouple locations are shown in (b). It may be noticed that there is a strong temperature variation in the gas from the top ($T_2 \simeq 55$ °C) to the bottom of the gas volume ($T_3 \simeq 37$ °C).

The pressure increase caused by sloshing motion is shown in Fig. A2a for the wave breaking case, $\omega/\omega_1 = 0.9817$, $A/R = 0.0227$ and the motionless interface. The corresponding temperature evolutions in the sloshing experiments are shown in Fig. A2b. The time origin corresponds here to the start of the forcing and is about 15 s after the end of the filling. The pressure increase without sloshing (thin solid curve in (a)) is caused by the molecular heat flux from the liquid to the interface. It serves as reference. As before, the evaporation rate q_v can be calculated from the rate of pressure increase using (4.5).

For the motionless regime we get from Fig. A1a a rate of pressure increase of $\partial p/\partial t \simeq 1.05$ mbar/s compared with $\partial p/\partial t \approx 38$ mbar/s in the case of sloshing. The gas temperature does not change significantly during the initial 20 s so that its contribution to $\partial p/\partial t$ may be neglected. For the motionless case we get from (4.5) $q_v = (\partial p/\partial t) \frac{V/S}{p_{vi}} \approx 0.024$ cm/s. The initial vapour density $\rho_{vi} = p_{vi}/r_v T_{gi} \simeq 2.3$ kg/m^3 and the boiling temperature $T_{si} \approx 280$ K, giving a Jacob number $Ja \approx -67$ when taking $T_{si} - T_{li} \approx -13$ K. The effective diffusion coefficient is calculated from (5.7) with $\delta_T \approx 3(4.45 \times 10^{-4} \times 300)^{1/2} \approx 1.1$ cm, giving $D_e \approx 3.94 \times 10^{-4}$ cm/^{2}s. This is close to the molecular value. However, evaporation causes surface cooling and hence a convectively unstable liquid surface layer [17,18]. The Rayleigh number $Ra = \frac{\alpha g \Delta T \delta^3}{D_T \nu}$, where α is the coefficient of volume expansion, and ΔT the temperature difference between the surface and the bulk liquid temperatures, is

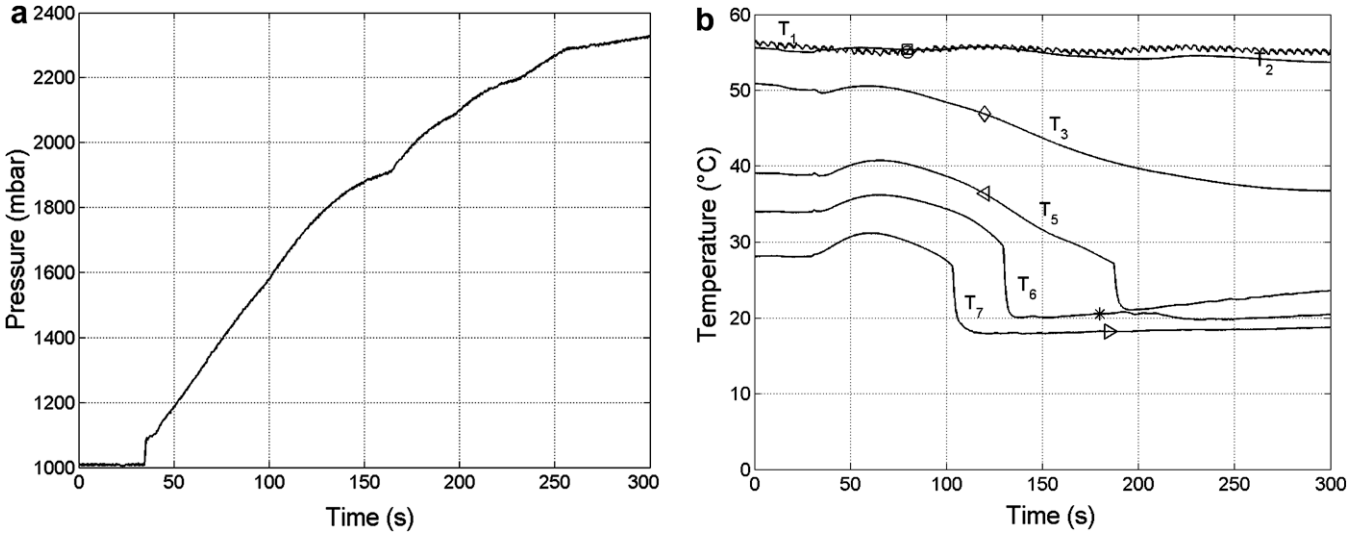

Fig. A1. (a) Pressure increase during liquid supply up to a height of 5.5 cm (5.5 cm liquid depth), (b) corresponding temperature variations.

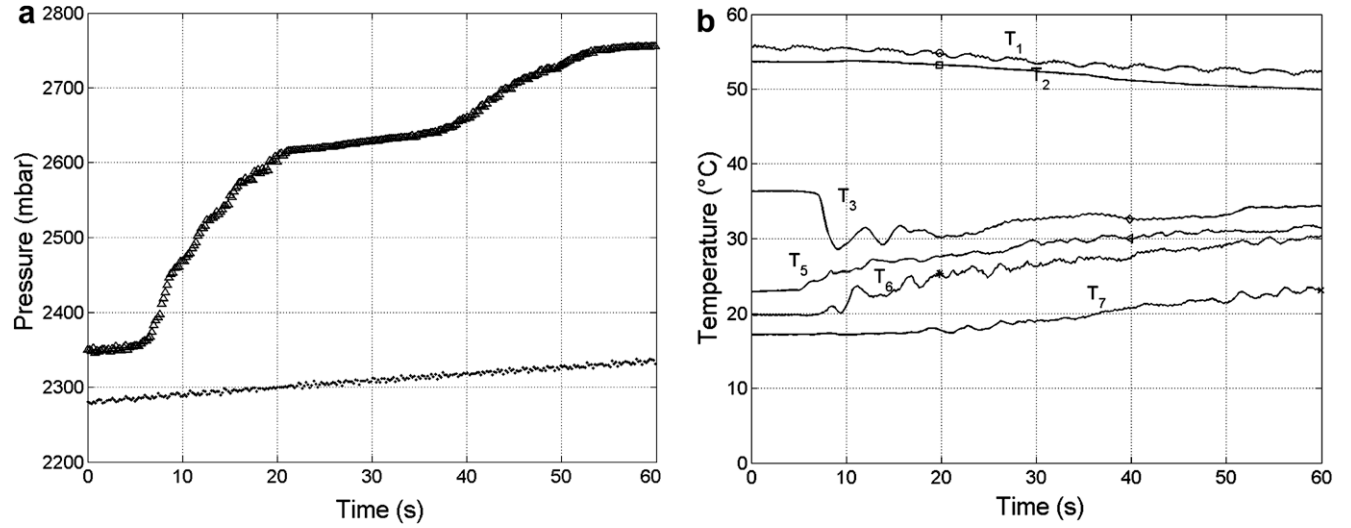

Fig. A2. Pressure (a) and temperature (b) evolutions as a function of time with the time origin corresponding to the start of container forcing; △ is the pressure increase with sloshing and the dotted line corresponds to the increase due to molecular diffusion.

large (order 10^7) so that a much larger heat flux and evaporation rate than by molecular diffusion alone would be expected. Observations show that this is not the case. A plausible explanation is that because the surface temperature is not imposed, it is likely that in the convectively unstable regime $\Delta T \ll |T_s - T_l|$.

For the sloshing regime where $\partial p/\partial t \approx 38$ mbar/s we get with $p_{vi} \simeq 375$ mbar, $T_{si} - T_{li} \approx -10$ K, $\rho_v \simeq 2.8$ kg/m^3 and $q_v \approx 0.59$ cm/s, $Ja \approx -43$. From (4.5) we get $q_v \approx 0.59$ cm/s and from (5.5) $D_e \approx 0.0147$ cm^2/s. The dimensionless value $D_e^* = D_e/(gR^3)^{1/2} \approx 42 \times 10^{-6}$.

The temperature evolutions with time are shown in Fig. A2b for the case with sloshing only (the evolutions without sloshing are of little interest). It is seen that the bulk liquid temperature (T_6 for example) increases substantially during the experiment of about 60 s. This is because the liquid is heated by the hot walls of the upper chamber as it moves up the wall during sloshing. Correspondingly the wall is cooled down. However, because the wall temperature is below the boiling temperature at the operating pressure $p > 2$ bar, there is no evaporation at the wall except near the leading edge of the wave. This contribution to the evaporation rate is likely to be small.

References

[1] T. Maruse, H.S. Wang, J.W. Rose, Marangoni condensation of steam-ethanol mixtures on a horizontal tube, Int. J. Heat Mass Transfer 50 (2007) 3754–3779.

[2] W.S. Huo, Y.M. Lie, Y.Y. Hsieh, T.F. Lin, Condensation heat transfer and pressure drop of refrigerant R-410A flow in a vertical plate heat exchanger, Int. J. Heat Mass Transfer 48 (2005) 5205–5220.

[3] F. Mayinger, S. Kakac, Turbulent film condensation on a horizontal tube with external flow of a pure vapour, Int. J. Heat Mass Transfer 41 (1998) 537–545.

[4] B. Jähne, H. Haussecker, Air–water gas exchange, Annu. Rev. Fluid Mech. 30 (1998) 443–468.

[5] E.M. Moran, N.B. McNeils, M.T. Kudlac, M.S. Haberbusch, G.A. Satornino, Experimental results of hydrogen slosh in a 60 cubic foot (1750 l) tank. 30th Joint Propulsion Conference, 1994.

[6] J. Lacapere, Results of the sloshing tests with LOX, AIR LIQUID Report No. RT-RE-22R22-0501-AIRL-01, 2005.

[7] H.N. Abramson, The dynamic behaviour of liquids in moving containers. NASA Publ. TR SP-106, 1966.

[8] R.A. Ibrahim, Liquid Sloshing Dynamics, Cambridge University Press, 2005.

[9] J.W. Miles, Resonantly forced surface waves in a circular cylinder, J. Fluid Mech. 149 (1984) 15–31.

[10] A. Royon-Lebeaud, E.J. Hopfinger, A. Cartellier, Liquid sloshing and wave breaking in circular and square-base cylindrical containers, J. Fluid Mech. 577 (2007) 467–494.

[11] O.M. Faltinsen, O.F. Rognebakke, I.A. Lukovsky, A.N. Timokha, Multidimensional modal analysis of nonlinear sloshing in a rectangular tank with finite water depth, J. Fluid Mech. 407 (2000) 201–234.

[12] O.M. Faltinsen, O.F. Rognebakke, A.N. Timokha, Resonant three-dimensional nonlinear sloshing in a square-base basin, J. Fluid Mech. 487 (2003) 1–42.

[13] S.P. Das, E.J. Hopfinger, Parametrically forced gravity waves in a circular cylinder and finite-time singularity, J. Fluid Mech. 599 (2008) 205–228.

[14] J.W. Miles, D.M. Henderson, Parametrically forced surface waves, Annu. Rev. Fluid Mech. 22 (1990) 143–165.

[15] G.I. Taylor, The instability of liquid surfaces when accelerated in the direction perpendicular to their planes, Proc. R. Soc. Lond. A 201 (1950) 192.

[16] E.J. Hopfinger, S.P. Das, Mass transfer enhancement by capillary waves at a liquid-vapour interface, Exp. Fluids (2008) in press.

[17] T.D. Foster, Onset of convection in a layer of fluid cooled from above, Phys. Fluids 8 (1965) 1770–1774.

[18] W.G. Spangenberg, W.R. Rowland, Convective circulation in water induced by evaporative cooling, Phys. Fluids 4 (1961) 743–750.